

IMECE2003-41084

SHAPE CONTROL OF A FLEXIBLE MIRROR USING AN ELECTRON GUN

Hartono Sumali¹, Jeffrey W. Martin²,
 Pavel Chaplya³, and James M. Redmond¹

P.O. Box 5800
 Albuquerque, NM 87185

Sandia National Laboratories

¹Structural Dynamics Research, MS 0557

²Mechanical Systems Engineering Design, MS 0980

³Material Mechanics Research, MS 0847

Phone: 505-844-7918

Fax: 505-844-0078

hsumali@sandia.gov

ABSTRACT

Mirrors made of PVDF film are being considered for lightweight transportation and deployment in space. An array of electrodes can be used to distribute charges over the PVDF film for active shaping of the mirrors. This paper presents the derivation of a matrix that enables calculation of the shape of the two-dimensional mirror for any given electron distribution. Finite element simulation shows good agreement with a theoretical example. Furthermore, if a desired shape is given, the required voltage distribution can be computed using the singular value decomposition. Experiments were done in a vacuum vessel, where an electron gun was used to actuate a PVDF bimorph to a desired shape. Dynamic shape control is attainable at low frequencies. At higher frequencies, still significantly below structural resonance, actuation lag and parasitic DC offset can be significant problems that require future research to solve.

NOMENCLATURE

A	Area, a symbol denoting domain of integration
A_i	Area of electrode segment, a symbol denoting domain of integration
B	Stiffness constant, N
D	Plate stiffness constant, Nm
E	Matrix of electric fields, V/m
E	Electric field along poled direction, V/m
h	Thickness of laminate, m
h_a	Thickness of actuator layer, m
I	Number of actuator segments
K	Number of modes to control

k	Mode number
k_{max}	Number of modes included in calculation
L_s	Strain energy plus actuation energy, J
M_λ	Line moment due to piezoelectric actuation, N.
m_k	number of half sinusoids of mode k in the x direction, no unit
n_k	number of half sinusoids of mode k in the y direction, no unit
P	Strain energy contribution, Eq. (7)
Q	Actuation matrix, Eq. (18)
R	Actuation matrix, Eq. (26)
R^+	Multiplier matrix from SVD (Eq. 49)
S	Singular value matrix from SVD
T	Stress, Pa
U	Left unitary matrix from SVD
U	Strain energy, J
V	Right unitary matrix from SVD
V	Applied voltage, V
W	Matrix of deflections, m
$w(x,y)$	Deflection, m
x	Lengthwise coordinate, m
Y	Young's modulus, Pa
y	Widthwise coordinate, m
z	Through-thickness coordinate, m
ϵ	Strain, dimensionless
ϵ_A	Strain due to piezoelectric actuation, dimensionless
ϵ_{tol}	Low threshold in SVD

Φ	Matrix of shape functions
ϕ	Shape function
η	Modal coefficient
$\hat{\eta}$	Desired modal coefficient
$\tilde{\eta}$	Achieved modal coefficient
λ	Wavelength of Light, m
ν	Poisson's ratio, dimensionless
σ	Singular value, component of S
σ_A	Stress due to piezoelectric actuation, Pa

Subscripts and superscripts

a	Pertaining to actuator layer
$analytical$	Computed analytically
FEM	Computed by FEM
k	Mode number
i	Segment number
T	Transpose
A	Resulting from piezoelectric actuation

Terms

Bimorph	Substrate with a PVDF layer on top and another PVDF layer on the bottom.
Lidar	Light ranging and detection
FEM	Finite Element Model
NGST	Next Generation Space Telescope
Pixel	Smallest unit area of control
PVDF	(PolyVinylidene Fluoride) a piezoelectric polymer
RMS	Root Mean Square
SVD	Singular Value Decomposition

1. INTRODUCTION

This paper discusses a thin film mirror made of a PVDF bimorph actuated by an electron gun. The motivation for the work is the advancement of low-mass space-based optical systems. The general trend in space-based optical systems is toward high performance at reduced system mass and launch volume. High performance translates directly to large aperture optical systems. This drives the need to package large diameter optics in packages small enough to stow atop a small booster rocket. NASA's immediate goal for NGST is a primary collector with an areal density of less than 15 kg/m². The NASA Gossamer initiative has the goal of 1 kg/m² primary mirrors.

Achieving these dramatic reductions in overall system launch size and mass while maintaining resolution and

sensitivity requires the development of very lightweight, large aperture space-based optics. While many researchers are considering on-orbit assembly of rigid optical mirror segments to circumvent geometric limitations imposed by launch vehicles, the cost penalties associated with their volumetric and weight constraints limit the aperture diameter to approximately 10 meters. Therefore, ultra large apertures will likely only be obtained using deployable thin-skin mirror technology. Ultra large deployable thin-skin mirrors may offer orders of magnitude improvement in resolution and sensitivity over what is achievable today, yet many technological barriers must be overcome to make this approach a viable alternative for future system designs.

Functional thin-film large aperture systems have the same surface tolerance requirements as any other optical system. Imaging systems today have surface qualities on the order of ten nanometers. Other light based concepts like Lidar systems have a more relaxed tolerance of 700nm RMS with 2.4 μ m peak to valley (Warren, 1990). Such tolerances are unlikely to be achieved by design and fabrication. Even if they were, disturbances will drive the mirrors out of tolerance. Therefore, active shape control is required for shape correction. In such control systems, a distributed array of actuators is needed. If conventional actuators such as piezoelectric stack pushers are used, then the large number of actuators in the array, the mass of the actuators and power supplies, and the bulk of cables to the actuators will defeat the purpose of light-weight reflectors.

Piezoelectric laminate actuators and electron guns offer a very attractive solution to this problem, having previously been demonstrated to selectively adjust discrete surface areas (Henson *et al.*, 2001). One electron gun can distribute charges over a wide array of piezoelectric patches on the reflector. The patches expand or contract according to the charges, thereby changing the shape of the reflector.

The idea of using piezoelectric actuators to control the shape of a thin film mirror has been explored for over a decade (Tabata *et al.*, 1992; Ueba *et al.*, 1994; Tabata and Natori, 1996; Paradies *et al.*, 1996; Chellabi *et al.*, 1997; Yoon and Washington, 1998; Paradies and Hertwig, 1999; Maji and Starnes, 2000). Electron guns have been shown to be effective in controlling one-dimensional piezoelectric laminates (Martin *et al.*, 2000). The work discussed in this paper extends the use of the electron gun to controlling the shape of two-dimensional piezoelectric laminates. The theory will be developed for flat plates. However, the application can be extended to shape correction of paraboloid and other common reflector shapes.

The presentation starts with a simplified analytical model that describes how electric fields create curvature in the thin film. A finite element analysis is then shown to support the analytical example. Finally, a laboratory experiment is presented to prove the concept of using an electron gun to create electric fields in the film. In this phase of the work, the

experiment was performed to assess the strengths and limitations of the electron-gun-actuated piezoelectric sheet mirror concept with dynamic control.

2. RELATIONSHIP BETWEEN SEGMENT VOLTAGE DISTRIBUTION AND LAMINATE DEFLECTION

Figure 1 is a sketch of the flexible mirror, which is modeled as three layers. The top and bottom layers are piezoelectric PVDF. The middle layer is a bonding layer made of material such as epoxy. The PVDF layers have silver electrodes with negligible thickness. The electrodes are segmented as shown in Figure 2. Each segment will be bombarded with electrons from an electron gun until a certain electric field is induced in the part of the laminate under the segment. This section presents a simplified method to predict the deflection of the laminate for any given distribution of segment voltage.

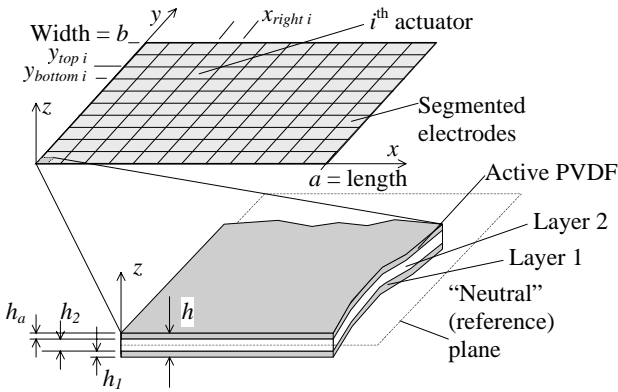


Figure 1 PVDF Bimorph with Segmented Electrodes

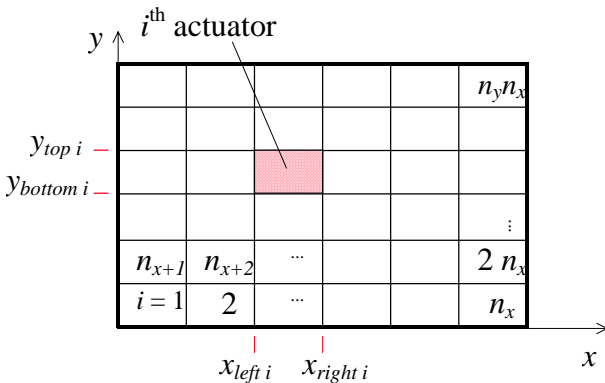


Figure 2 Electrode Segment Numbering system. n_x = number of segments in the x direction; n_y = number of segments in the y direction.

The deflection of the laminate is assumed to be a linear combination of basis functions

$$w(x, y) = \sum_{k=0}^{\infty} \phi_k(x, y) \eta_k \quad (1)$$

where the set of ϕ_k forms a basis of admissible functions for the boundary conditions. For example, if all four edges of the laminate are simply supported, then we can use

$$\phi_{mn}(x, y) = \sin(m\pi x/a) \sin(n\pi y/b) \quad (2)$$

where m and n are the number of half sinusoids in the lengthwise and the widthwise direction, respectively. The basis functions in this paper will be called the *mode shape* functions. (This term is borrowed from dynamics even though this section will not consider dynamic effects.) In a two-dimensional structure like the rectangular laminates considered here, the mode shapes have two indices m and n . To shorten the notation and facilitate derivation, m and n are collapsed into one index k in ascending order of the natural frequency that would result if the laminate vibrated in mode (m, n) . This renumbering method is shown in Fig. 3 for a particular aspect ratio. For example, for $k = 1$, the corresponding m_k and n_k are 1 and 1, respectively. For $k = 4$, the corresponding m_k and n_k are 3 and 1, respectively, and so on as illustrated in Fig. 3.

k	m	n	ω_k rad/s	$\phi_k(x, y)$	k	m	n	ω_k rad/s	$\phi_k(x, y)$
1	1	1	17		4	3	1	59	
2	2	1	33		5	2	2	69	
3	1	2	53		6	3	2	95	

Figure 3 Reducing mode indices m, n into one index k .

The strain energy in the laminate when the laminate is deflected as above is

$$U = \frac{1}{2} \int_0^a \int_0^b \int_{-h/2}^{h/2} \boldsymbol{\epsilon}^T \mathbf{T} dz dy dx \quad (3)$$

Under the Kirchoff-Love assumption (Soedel, 1993), the strain can be expressed in terms of the curvatures

$$\boldsymbol{\epsilon} = -z \left(\frac{\partial^2 w}{\partial x^2} \quad \frac{\partial^2 w}{\partial y^2} \quad 2 \frac{\partial^2 w}{\partial x \partial y} \right)^T \quad (4)$$

If the Poisson's ratios of all the laminae are approximately equal, the stress can be related to the strain by

$$\mathbf{T} = \frac{Y}{1-\nu^2} \begin{bmatrix} 1 & \nu & 0 \\ \nu & 1 & 0 \\ 0 & 0 & \frac{1-\nu}{2} \end{bmatrix} \boldsymbol{\varepsilon} \quad (5)$$

Substitution of Eq. (4) and Eq. (5) into Eq. (3) results in the strain energy contribution of mode- k

$$P_k = \int_A \frac{\left(\frac{\partial^2 \phi_k(x,y)}{\partial x^2} \quad \frac{\partial^2 \phi_k(x,y)}{\partial y^2} \quad 2 \frac{\partial^2 \phi_k(x,y)}{\partial x \partial y} \right)}{1-\nu^2} \begin{bmatrix} 1 & \nu & 0 \\ \nu & 1 & 0 \\ 0 & 0 & \frac{1-\nu}{2} \end{bmatrix} \begin{bmatrix} \frac{\partial^2 \phi_k(x,y)}{\partial x^2} \\ \frac{\partial^2 \phi_k(x,y)}{\partial y^2} \\ 2 \frac{\partial^2 \phi_k(x,y)}{\partial x \partial y} \end{bmatrix} dA \quad (6)$$

which evaluates to

$$P_k = \frac{1}{1-\nu^2} \int_A \left\{ \left(\frac{\partial^2 \phi_k(x,y)}{\partial x^2} \right)^2 + \left(\frac{\partial^2 \phi_k(x,y)}{\partial y^2} \right)^2 + 2\nu \frac{\partial^2 \phi_k(x,y)}{\partial x^2} \frac{\partial^2 \phi_k(x,y)}{\partial y^2} + 2(1-\nu) \left(\frac{\partial^2 \phi_k(x,y)}{\partial x \partial y} \right)^2 \right\} dA \quad (7)$$

The resistance of the panel to bending can be defined with a *plate stiffness* constant

$$D = \int_{z=-h/2}^{h/2} Y(z) z^2 dz \quad (8)$$

The strain energy can now be expressed in terms of Eq. (1) and Eq. (6)

$$U = 0.5D \sum_{k=1}^{\infty} P_k \eta_k^2 \quad (9)$$

The above equation expresses the strain energy in the deflected laminate in terms of "modal coordinates" η_k , the plate stiffness D , and a set of constants P_k that depends on the "mode shapes" ϕ_k .

The actuation from the piezoelectric material can be modeled as an induced bending moment (Crawley and de Luis, 1987)

$$\mathbf{M}_\Lambda = \int_{piezo} \boldsymbol{\sigma}_\Lambda z dz \quad (10)$$

where *piezo* denotes that the integration is to be done only over the lamina that has piezoelectric action. The actuated stress $\boldsymbol{\sigma}_\Lambda$ is related to the actuation strain $\boldsymbol{\varepsilon}_\Lambda$ by

$$\boldsymbol{\sigma}_\Lambda = \frac{Y}{1-\nu^2} \begin{bmatrix} 1 & \nu & 0 \\ \nu & 1 & 0 \\ 0 & 0 & \frac{1-\nu}{2} \end{bmatrix} \boldsymbol{\varepsilon}_\Lambda \quad (11)$$

The actuation strain $\boldsymbol{\varepsilon}_\Lambda$ is a product of the piezoelectric constant and the applied electric field

$$\boldsymbol{\varepsilon}_\Lambda = \begin{bmatrix} d_{31} \\ d_{32} \\ 0 \end{bmatrix} E \quad (12)$$

where the electric field is the voltage divided by the thickness of the actuator layer

$$E_i = V_i / h_a \quad (13)$$

In the above three equations, it has been assumed that the piezoelectric effects are linear. This assumption is valid over a broad range of excitation. The actuation moment in Eq. (10) can also be written as

$$\mathbf{M}_\Lambda = \int_{piezo} \frac{Y}{1-\nu^2} \begin{bmatrix} 1 & \nu & 0 \\ \nu & 1 & 0 \\ 0 & 0 & \frac{1-\nu}{2} \end{bmatrix} \begin{bmatrix} d_{31} \\ d_{32} \\ 0 \end{bmatrix} E z dz \quad (14)$$

The strain energy in the laminate under actuator segment i (Figure 2) is

$$E_A(i) = \int_{A_i} \boldsymbol{\kappa}^T \mathbf{M}_\Lambda(i) dA \quad (15)$$

where $\boldsymbol{\kappa}$ is the curvature of the deflection from Eq. (1)

$$\boldsymbol{\kappa} = - \sum_{k=1}^{\infty} \begin{pmatrix} \frac{\partial^2 \phi_k(x, y)}{\partial x^2} \\ \frac{\partial^2 \phi_k(x, y)}{\partial y^2} \\ 2 \frac{\partial^2 \phi_k(x, y)}{\partial x \partial y} \end{pmatrix} \eta_k \quad (16)$$

(Membrane forces are excluded from Eq. (15) because their contribution to strain energy is negligible (Tzou and Fu, 1994), especially for bimorph symmetric actuation.) Inspection of Eq. (14), (15) and (16) suggests that a constant can be defined to save space in writing the expression for the effect of actuator segment i on deflection mode k . This constant is

$$\mathbf{Q}_{ki} = \int_{A_i} \frac{\left(\frac{\partial^2 \phi_k(x, y)}{\partial x^2} \quad \frac{\partial^2 \phi_k(x, y)}{\partial y^2} \quad 2 \frac{\partial^2 \phi_k(x, y)}{\partial x \partial y} \right)}{1 - \nu^2} \begin{bmatrix} 1 & \nu & 0 \\ \nu & 1 & 0 \\ 0 & 0 & \frac{1 - \nu}{2} \end{bmatrix} \begin{pmatrix} d_{31} \\ d_{32} \\ 0 \end{pmatrix} dA \quad (17)$$

or, after multiplying out,

$$\mathbf{Q}_{ki} = \int_{A_i} (d_{31} + \nu d_{32}) \frac{\partial^2 \phi_k}{\partial x^2} + (d_{32} + \nu d_{31}) \frac{\partial^2 \phi_k}{\partial y^2} dA \quad (18)$$

To save space in writing expressions of strain energies, define an ‘‘actuator stiffness’’ constant similar to the one in Eq. (8)

$$B = \int_{piezo} Y(z) z dz \quad (19)$$

The above constant quantifies how stiff the actuator is to work against the stiffness D of the entire laminate. With the above notation, the actuation energy of actuator segment i can be written concisely as

$$E_A(i) = -BE_i \sum_{k=1}^{k_{\max}} \mathbf{Q}_{ki} \eta_{ki} \quad (20)$$

Consider only the part of the laminate that is covered by actuator i . The strain energy in that part, from Eq. (9), is

$$U(i) = 0.5D \sum_{k=1}^{k_{\max}} P_k \eta_{ki}^2 \quad (21)$$

In this part of the laminate, the sum of the strain energy and the actuation energy is

$$L_s(i) = U(i) + E_A(i) \quad (22)$$

Substituting Eq. (20) and (21) to the above equation results in

$$L_s(i) = 0.5D \sum_{k=1}^{k_{\max}} P_k \eta_{ki}^2 - BE_i \sum_{k=1}^{k_{\max}} \mathbf{Q}_{ki} \eta_{ki} \quad (23)$$

The k^{th} modal coefficient resulting from the actuation by the i^{th} segment, denoted by η_{ki} , can therefore be determined by minimizing $L_s(i)$ with respect to η_{ki} . Zeroing the derivative of $L_s(i)$ with respect to η_{ki} results in

$$\frac{\partial L_s(i)}{\partial \eta_{ki}} = DP_k \eta_{ki} - B\mathbf{Q}_{ki} E_i = 0 \quad (24)$$

Therefore, the k^{th} modal coefficient resulting from the actuation by the i^{th} segment is

$$\eta_{ki} = R_{ki} E_i \quad (25)$$

where

$$R_{ki} = \frac{B \mathbf{Q}_{ki}}{D P_k} \quad (26)$$

The last two equations and Eq. (1) enable us to calculate how much deflection will be realized by actuator segment i with a given electric field E_i .

$$w_i(x, y) = \sum_{k=0}^{k_{\max}} \phi_k(x, y) \eta_{ki} \quad (27)$$

where η_{ki} is from Eq. (25). The total deflection due to all actuators can be obtained by superposition.

$$w(x, y) = \sum_{i=1}^{i_{\max}} w_i(x, y) \quad (28)$$

or, substituting Eq. (25) and (27) into the last equation,

$$w(x, y) = \sum_{i=1}^{i_{\max}} \sum_{k=1}^{k_{\max}} \phi_k(x, y) \mathbf{R}_{ki} E_i \quad (29)$$

Thus, in matrix notation, the deflection caused by the actuator electric field distribution \mathbf{E} is

$$w(x, y) = \mathbf{\Phi}^T(x, y)\mathbf{R}\mathbf{E} \quad (30)$$

where the mode shape matrix $\mathbf{\Phi}$ is

$$\mathbf{\Phi} = \begin{bmatrix} \phi_1(x, y) \\ \vdots \\ \phi_k(x, y) \\ \vdots \\ \phi_{k_{\max}}(x, y) \end{bmatrix} \quad (31)$$

Matrix \mathbf{R} is composed of the ki components from Eq. (26). Vector \mathbf{E} contains the electric fields of the actuators according to the actuator numbering method shown in Fig. 2.

3. NUMERICAL EXAMPLE OF ACTUATION

As an example, consider a three-layer laminate shown in Fig. 1, with the following properties: Length $a = 71$ mm; width $b = 71$ mm; number of segments lengthwise = 2; number of segments widthwise = 2; Thickness: PVDF layers $h_a = 52\mu\text{m}$; Epoxy bonding layer $h_2 = 28\mu\text{m}$; Young's moduli: PVDF layers $Y_a = 2.9(10)^9$ Pa; Epoxy bonding layer $Y_2 = 1.06(10)^9$ Pa; Poisson's ratio $\nu = 0.35$ for all layers; Piezoelectric constants $d_{31} = d_{32} = 23(10)^{-12}$ m/V. The laminate is simply supported along all four edges. The actuator segments are energized with a voltage distribution shown in Fig. 4(a).

The theory developed in the previous section will now be used to calculate the resulting deflection of the laminate. The plate stiffness according to Eq. (8) and Fig. 1 is

$$D = \int_{-(h_2/2+h_a)}^{h_2/2+h_a} Y(z) z^2 dz = 2Y_a \int_{h_2/2}^{h_2/2+h_a} z^2 dz + Y_2 \int_{-h_2/2}^{h_2/2} z^2 dz \quad (32)$$

or, after the integration,

$$D = \frac{Y_2 h_2^3}{12} + Y_a h_a \left[\frac{h_2^2}{2} + h_2 h_a + \frac{2h_a^2}{3} \right] \quad (33)$$

In the bimorph laminate that we use here, the voltage in the lower actuator layer is equal and opposite to the voltage in the upper actuator layer. Therefore, the two piezoelectric layers reinforce each other's bending actuation, and the B constant in Eq. (19) is

$$B = - \int_{-(h_2/2+h_a)}^{-h_2/2} Y(z) z dz + \int_{h_2/2}^{h_2/2+h_a} Y(z) z dz \quad (34)$$

where the domain of the integration includes both piezoelectric actuator layers. The above integration results in

$$B = Y_a h_a (h_2 + h_a) \quad (35)$$

The matrix \mathbf{Q} is calculated by inserting the mode shape function for the simply supported laminate,

$$\phi_k = \sin(m_k \pi x / a) \sin(n_k \pi y / b) \quad (36)$$

into Eq. (18). This results in

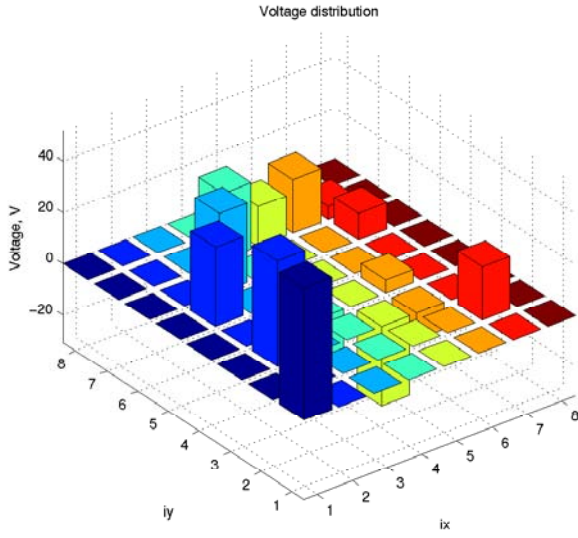
$$\mathbf{Q}_{ki} = \frac{-1}{abm_k n_k} \left\{ \left[b^2 m_k^2 (d_{31} + \nu d_{32}) + a^2 n_k^2 (d_{32} + \nu d_{31}) \right] \left\{ \cos(m_k \pi x_{\text{right } i} / a) - \cos(m_k \pi x_{\text{left } i} / a) \right\} \left\{ \cos(n_k \pi y_{\text{top } i} / b) - \cos(n_k \pi y_{\text{bottom } i} / b) \right\} \right\} \quad (37)$$

for each mode k and actuator number i . Edge positions $x_{\text{right } i}$, $x_{\text{left } i}$, $y_{\text{top } i}$, and $y_{\text{bottom } i}$ are as shown in Fig. 2. Likewise, \mathbf{P} is calculated by inserting the mode shape function into Eq. (7)

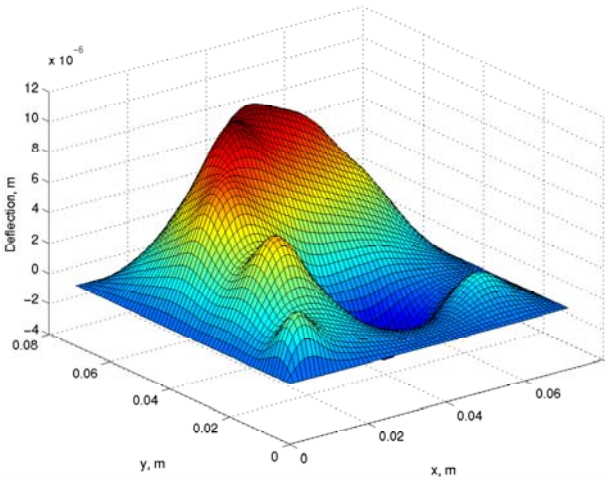
$$P_k = \frac{\pi^4}{4(1-\nu^2)} \frac{(a^2 n_k^2 + b^2 m_k^2)}{a^3 b^3} \quad (38)$$

Next, the \mathbf{R} matrix is calculated from Eq. (26). Finally, the deflection of the laminate is computed using (30).

The resulting deflection is shown in Fig. 4(b). Observation of the actuator voltage distribution in Fig. 4(a) and the resulting deflection in Fig. 4(b) suggests that the curvature of the deflection under each actuator segment is roughly proportional to the voltage in that segment. This agrees with the formulation that the piezoelectric actuators create deflection by inducing curvature. The product $B\mathbf{Q}$ in Eq. (27) is a measure of the actuator authority. The product $\mathbf{P}\mathbf{R}$ is a measure of the structure's resistance to bending.



(a)



(b)

Figure 4 Electrode Voltage Distribution and Resulting Shape.

4. CALCULATING VOLTAGE DISTRIBUTION FOR A DESIRED DEFLECTION SHAPE

The above example shows that the deflection for a given electrode electric field (or voltage) distribution can be computed relatively easily. In the practical application, the laminate is designed to control the shape of a mirror by energizing the actuator segments with electric fields. Therefore, the important problem is how to determine the required voltage distribution to achieve a desired shape. This

problem is the inverse of the actuation problem solved in section 2. As an example, let it be desired to shape the mirror into a certain deflected shape that can be expressed in terms of sinusoidal basis functions as

$$\begin{aligned}
 w(x, y) = & 10^{-6} [3 \sin(\pi x / a) \sin(\pi y / b) \\
 & - 2 \sin(2\pi x / a) \sin(\pi y / b) \\
 & + \sin(\pi x / a) \sin(2\pi y / b) \\
 & + 0.5 \sin(2\pi x / a) \sin(2\pi y / b)]
 \end{aligned} \quad (39)$$

The transformation of the deflection function from physical coordinates into the "modal" coordinate could be done by several techniques such as two-dimensional Fourier series. In the above example, the deflection shape can be expressed as the modal coefficients, *i.e.*,

$$\hat{\eta} = 10^6 [3 \quad -2 \quad 1 \quad 0 \quad 0.5 \quad 0 \quad 0 \quad \dots] \quad (40)$$

We would like to determine the actuator voltage distribution that results in the above shape.

Equations (25) and (26) show that the modal coefficients resulting from an electric field distribution \mathbf{E} is

$$\tilde{\eta} = \mathbf{R} \mathbf{E} \quad (41)$$

$k_{\max} \times 1 \quad k_{\max} \times i_{\max} \quad i_{\max} \times 1$

where k_{\max} is the number of modal coefficients to control, and i_{\max} is the number of actuator segments. If $k_{\max} = i_{\max}$, then the electric field distribution vector can be obtained by simply inverting \mathbf{R}

$$\mathbf{E} = \mathbf{R}^{-1} \hat{\eta} \quad (42)$$

In general, k_{\max} is not equal to i_{\max} . The best set of electric fields (hence actuator voltages) can be solved for by minimizing the least-squares difference between the desired modal coefficients and the achievable modal coefficients

$$\begin{aligned}
 J & \equiv [\hat{\eta} - \mathbf{R}\mathbf{E}]^T [\hat{\eta} - \mathbf{R}\mathbf{E}] \\
 & = \hat{\eta}^T \hat{\eta} - 2\hat{\eta}^T \mathbf{R}\mathbf{E} + \mathbf{E}^T \mathbf{R}^T \mathbf{R}\mathbf{E}
 \end{aligned} \quad (43)$$

Setting

$$\frac{\partial J}{\partial \mathbf{E}} = [0 \quad \dots \quad 0]_{i \times i_{\max}} \quad (44)$$

results in the normal equations, which means that the electric field distribution could be obtained by

$$\mathbf{E} = [\mathbf{R}^T \mathbf{R}]^{-1} \mathbf{R}^T \hat{\eta} \quad (45)$$

However, the product in the square bracket is usually ill conditioned. Therefore, normal equations often result in large computational errors. An example of enormous computational error is shown in Fig. 5.

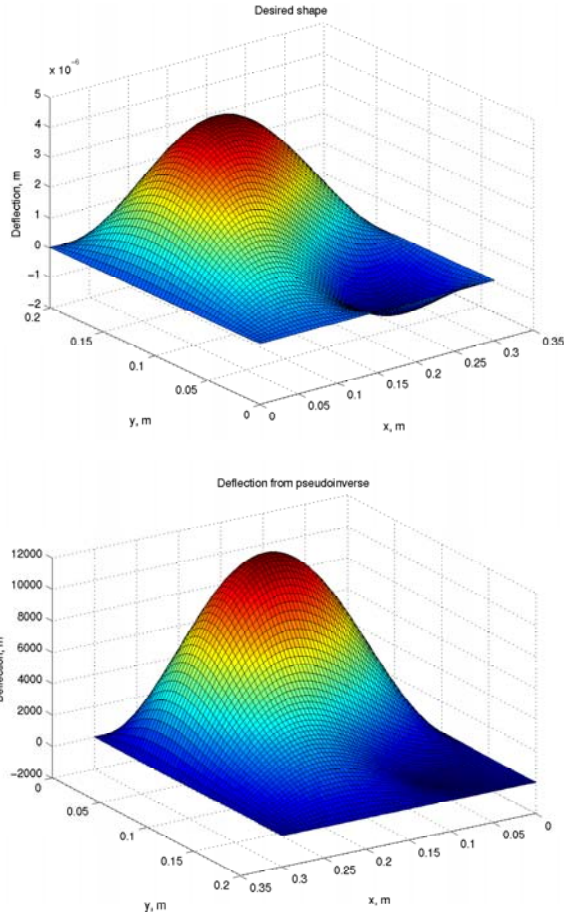


Figure 5 Enormous Error Resulting from Normal Equations.

One way to solve the above problem is the Singular Value Decomposition (SVD). With this method, the \mathbf{R} matrix is decomposed into

$$\mathbf{R} = \mathbf{U} \mathbf{S} \mathbf{V} \quad (46)$$

where \mathbf{U} and \mathbf{V} are unitary matrices, and the diagonal rectangular matrix

$$\mathbf{S} = \begin{bmatrix} \sigma_1 & 0 & \cdots & 0 \\ 0 & \sigma_2 & \cdots & 0 \\ \vdots & \vdots & \ddots & \vdots \\ 0 & 0 & \cdots & \sigma_{i_{\max}} \\ & & & \mathbf{0} \end{bmatrix} \quad (47)$$

contains the singular values. From the above three matrices, we compute another matrix

$$R^+_{ik} = \sum_{\text{all } j \text{ where } \sigma_{jj} > \varepsilon_{tol}} \frac{V_{ij} U_{kj}}{\sigma_{jj}} \quad (48)$$

The threshold ε_{tol} can be determined numerically by inspection from the computation. Finally, the electric field distribution can be obtained by

$$\mathbf{E} = \mathbf{R}^+ \hat{\boldsymbol{\eta}} \quad (49)$$

The SVD technique is applied to the problem shown in Fig. 5, in which normal equations had caused enormous error. The voltage distribution resulting from SVD is shown in Fig. 6(b). The resulting deflection shape shown in Fig. 6(c) is very close to the desired deflection shape in Fig. 6(a).

5. COMPARISON WITH FINITE ELEMENT MODELS

Numerical methods have been used in previous work to calculate laminate deflection due to segmented piezoelectric actuators. (For example, Agrawal *et al.* (1994) developed a finite difference solution to the problem.) In this paper, we constructed a finite element model with ANSYSTM according to the numerical example presented in Section 3. The Epoxy bonding layer in that example is 71 mm long but only 28 μm thick. Piezoelectric elements are available in ANSYSTM as solid elements and not as plate or shell elements. To keep the aspect ratio of all elements between 1 and 2, a very fine mesh was therefore created even though the geometry of the model is very simple. The voltage distribution in Fig. 7(a) is applied to the piezoelectric elements corresponding to the segments.

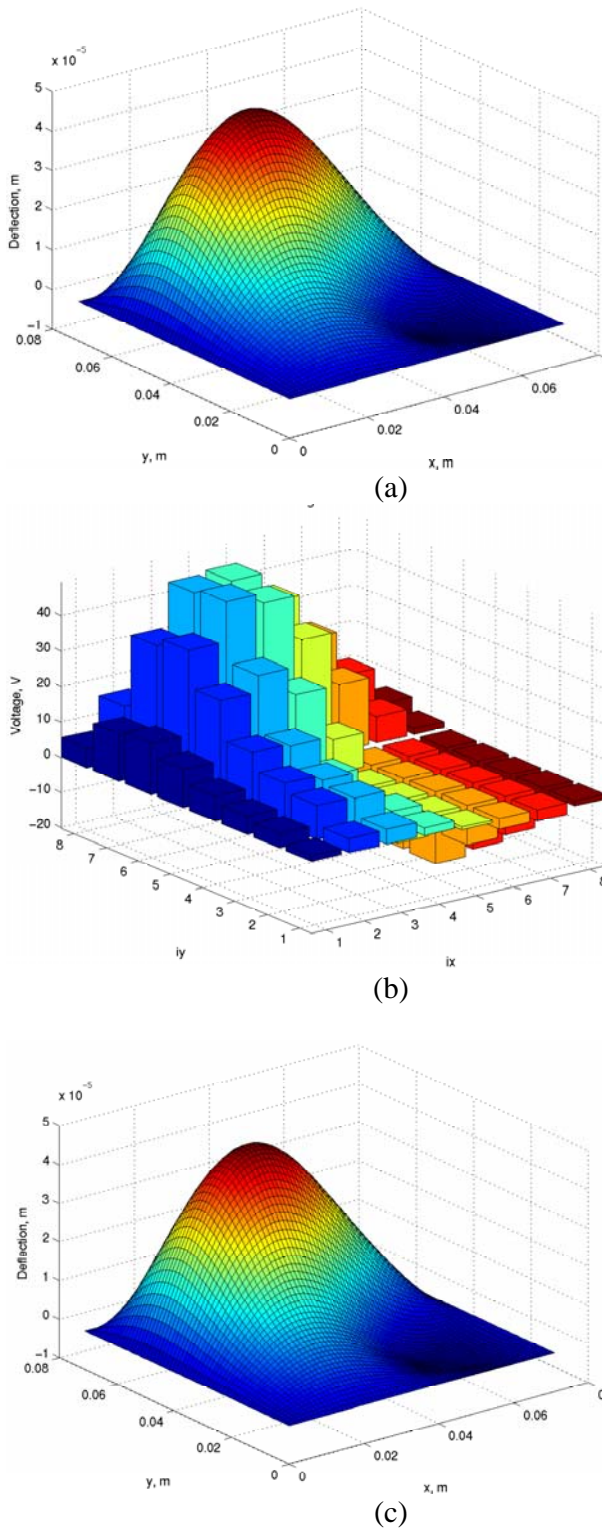


Figure 6 Desired Shape, Voltage Distribution, and Achieved Shape.

The resulting actuated shape is shown in Fig. 7(b). The corresponding analytical shape computed with the technique in Section 4 is shown in Fig. 7(c). The maximum deflection computed by the theoretical method is 5.7% larger than the maximum deflection computed by FEM. The similarity between the shapes of the deflections can be quantified by the “cosine of the angle” between the deflection matrices, expressed as

$$\cos(\theta) = \frac{\text{tr}(\mathbf{W}_{analytical}^T \mathbf{W}_{FEM})}{\sqrt{\text{tr}(\mathbf{W}_{analytical}^T \mathbf{W}_{analytical}) \text{tr}(\mathbf{W}_{FEM}^T \mathbf{W}_{FEM})}} \quad (50)$$

This cosine will be unity if one matrix is a scalar multiple of the other, and zero if the two matrices are orthogonal. For the deflections in Fig. 7 with a grid of 32×32 points, $\cos(\theta) = 0.95$, which means that the deflection shape computed by the analytical method is very similar to the deflection shape computed by FEM.

6. EXPERIMENTAL ACTUATION WITH ELECTRON GUN

The voltage or electric field for controlling the shape of the thin mirror will be applied with an electron gun that deposits electrons on the mirror's electrode segments. Previous work by Henson *et al.* (2001) and Martin *et al.* (2001) have shown the feasibility of this electron-gun-actuation concept and the success in using it to control quasi-static tip displacement of cantilever beams. Similar experiments were performed in this work to characterize the dynamics of PVDF bimorph under electron gun excitation. Although the theory developed above was for static actuation, the experiments described below were done to gain some insight into dynamic actuation with an electron gun.

6.1 Experiment Setup

Figure 8 is a schematic of the experiment setup. The major components of the experiment setup were a computer controller, a Keyence LK-2503 laser displacement sensor, an XYZ staging system, an electron gun, a power amplifier, and the PVDF bimorph. The PVDF bimorph and the electron gun were kept inside a vacuum chamber (about 10^{-7} torr). The Keyence sensor was used to take point displacement measurements of the bimorph through a window on the chamber. (Although insufficient for the intended application, the $10\text{-}\mu\text{m}$ measurement resolution of the Keyence sensor was adequate for demonstration purposes.) The displacement sensor and the XYZ staging system were programmed to map the electron-actuated deflection profiles of the PVDF bimorph.

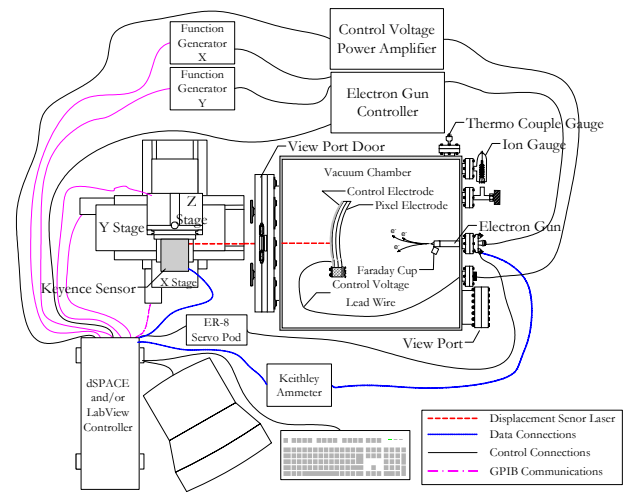
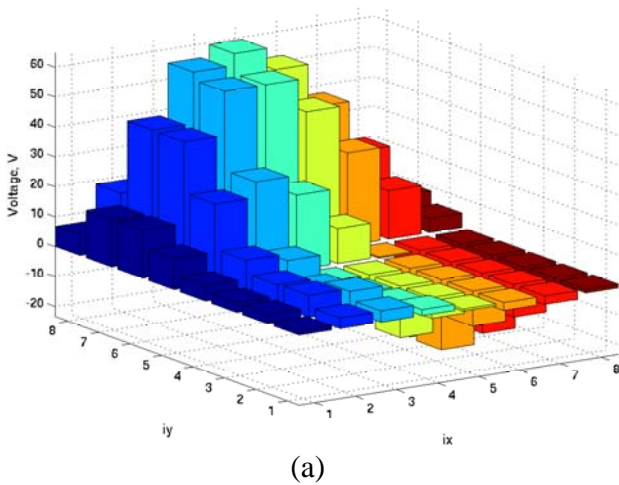


Figure 8 Setup for Electron Gun Experiment.

The computer positioned the Keyence sensor relative to the bimorph through adjustments of the XYZ staging system. The deflection profile of the entire bimorph was mapped by coordinating the x - y position of the measurement system with the measured bimorph deflection (in the z direction) at that position.

The electrodes covering the segments (called the *pixel electrodes*) of the bimorph receive a bombardment of electrons one electrode at a time. The energy level of the electron gun is kept constant for all segments. The flip side of the bimorph, where there is no electron bombardment, is covered entirely with a single *back-voltage electrode*. The *back voltage* from this electrode determines the electric field across the thickness of the bimorph in each targeted segment. The back voltage is controlled with a power amplifier. The net electric field in each segment is the electric field caused by the bombarding electrons minus the control field caused by the back voltage. Once the electron gun leaves pixel electrode number i to shoot the next electrode, the electric field across the thickness of segment i is locked in. Changing the back voltage for the next electrode does not alter the electric field in segment i . This electric field is unaffected by the change in the back voltage because there is neither deposition nor dissipation of electrons to or from the segment unless the segment is bombarded by electrons from the gun. The back voltage can be varied into positive or negative values.

The electron gun and its power amplifier and the back voltage electrode were adjusted remotely through the computer. All these experiments were conducted in vacuum to prevent scattering of the electron stream and unintended dissipation of electrons from the bimorph.

A 60 mm x 60 mm bimorph was mounted as a cantilever beam and actuated using a constant electron stream of 800 eV electrons at 13.95 μ Amps. The Keyence sensor was used to measure real-time displacements of the bimorph at the tip

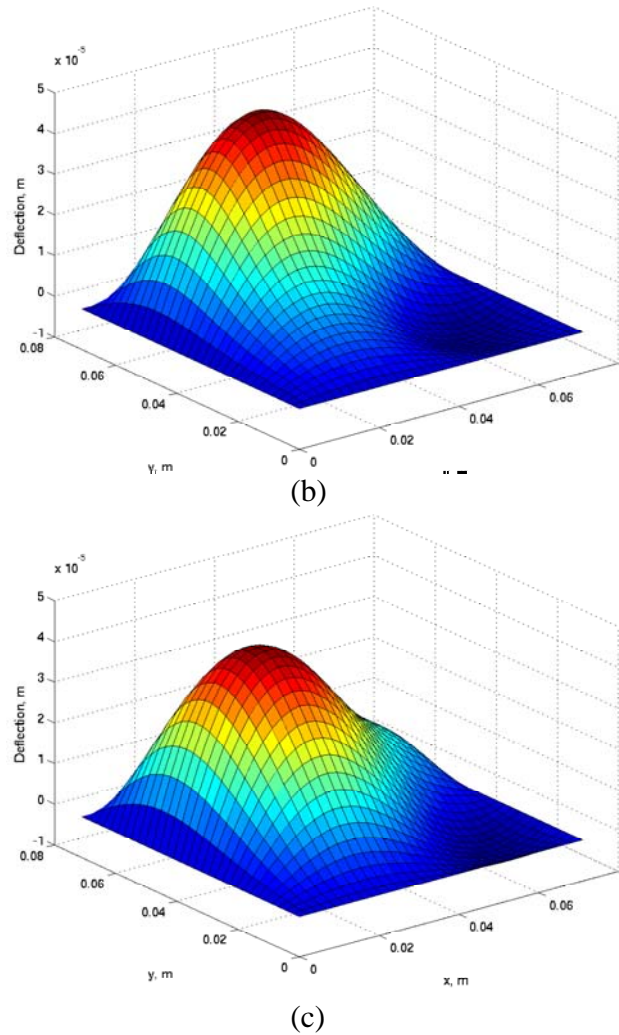


Figure 7 Finite Element Calculation of Deflection.

only. Sinusoidal voltages at frequencies ranging from 0.01 Hz to 5 Hz and amplitudes of 10 V to 500 V were used to vary the potential on the back electrode. The fundamental natural frequency of the beam is approximately 20 Hz. Therefore, mechanical resonance had little effect, and the dynamics of the cantilever bimorph was determined mainly by the dynamics of the electron gun actuation.

6.2 Experiment Result

Figure 9 shows the tip displacement control response of the cantilever. The response shown is linear for higher amplitude control inputs at all frequencies. Overall response magnitudes decrease with an increase in control input frequency. At low frequency (< 0.5 Hz) the system exhibits flat response across the range of control amplitudes. Figure 10 shows the phase lag response for the same experiment. As seen previously the lag response seems linear across the range of control amplitudes for all frequencies. This is shown in their flat response across the range of input amplitudes. As expected higher input frequencies induce higher phase lag.

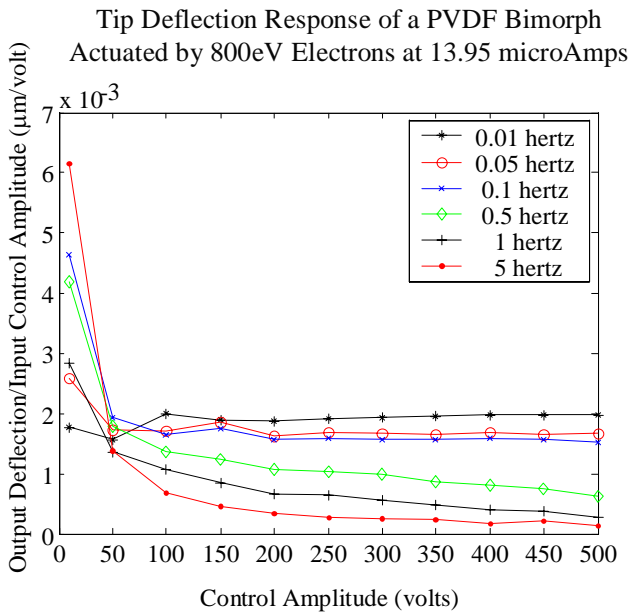


Figure 9 Dynamic Effect of Frequency on Deflection Amplitude.

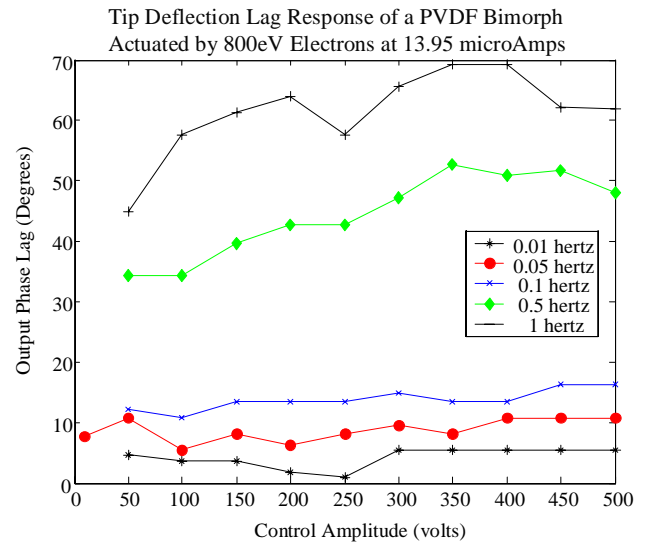


Figure 10 Phase Lag versus Amplitude.

Further examination shows a strong correlation between the system’s “DC offset” actuation and the amplitude responses. As the system responds to a sinusoidal control input, the deflection oscillates about a DC offset that appears to be related to the input frequency. Figure 11 shows transitions from large oscillations with little DC offset, to small oscillations (almost zero amplitude) with high DC offset as the control frequency increases. In dynamic control, this phenomenon might limit the control bandwidth to about 0.1 Hz. In the case of a large mirror application, each adjustment of the pixel-sized control area would be at this frequency. To maintain steady state in a large mirror, the overall refresh rate across all the thousands of control pixels would be much higher.

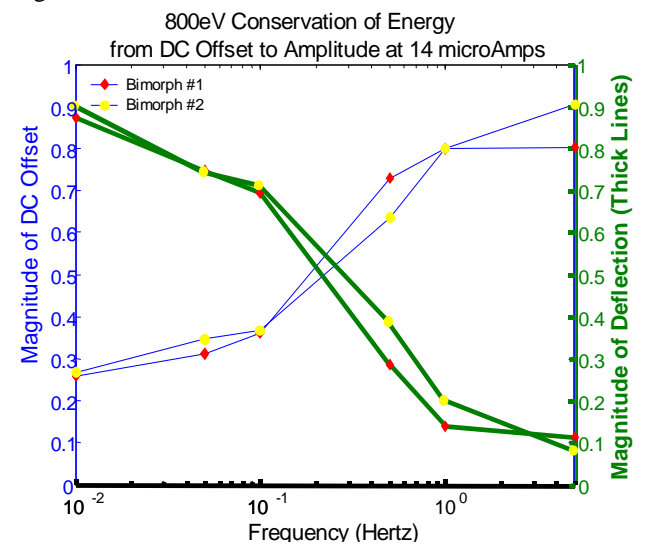


Figure 11 Effects of Frequency on Offset and Deflection.

7. CONCLUSIONS

The theory developed here for the two-dimensional actuation of bimorphs with piezoelectric segments and electron-gun excitation has been verified with finite element analysis. Preliminary laboratory experiments explored the dynamics of the electron gun actuation.

Control of the pixel bimorph concept is possible at low-frequency (0.05Hz). Overall the bimorph responds linearly to low-frequency input. As expected, response lag increases with frequency. It was also shown that higher frequencies caused larger DC offsets. Operating at low frequency minimizes both the DC offset and the response-lag, and maximizes the output amplitude response. Further research is needed before successful dynamic control can be done on the bimorph mirror.

8. ACKNOWLEDGMENT

This work was conducted at Sandia National Laboratories. Sandia is a multi-program laboratory operated under Sandia Corporation, a Lockheed Martin Company, for the United States Department of Energy under Contract DE-AC04-94-AL85000.

9. REFERENCES

- Agrawal, S. K., Tong, D-Q., and Nagaraja, K., 1994, "Modeling and shape control of piezoelectric actuator embedded elastic plates", *Journal of Intelligent Material Systems & Structures*, v 5 n 4 Jul. p 514-521.
- Chellabi, A. Stepanenko, Y. Dost, S., 1997, "Active shape control of a deformable mirror in an adaptive optics system", *Proceedings of the 1997 6th IEEE Pacific Rim Conference on Communications, Computers and Signal Processing*, Part 2 (of 2). Victoria, Can. Aug. 20-22.
- Crawley, E.F., and de Luis, J., 1987, "The Use of Piezoelectric Actuators as Elements of Intelligent Structures", *AIAA Journal*, v 25 n 10.
- Henson, T. D., Wehlburg, J. C., Redmond, J. M, Main, J. A., Martin, J. W., 2001, "Thin-Skin Deployable Mirrors for Remote Sensing Systems", *Sandia National Laboratories Report*, #SAND2001-0101, January.
- Maji, A K. Starnes, M A., 2000, "Shape measurement and control of deployable membrane structures", *Experimental Mechanics*, v 40 n 2 2000 p 154-159.
- Martin, J. W., Redmond, J. M., Barney, P. S., Henson, T. D., Wehlburg, J. C., Main, J. A., 2000, "Distributed sensing and shape control of piezoelectric bimorph mirrors", *Journal of Intelligent Materials and Smart Structures*, v 11 n 10 p 744-757.
- Martin, J. W, 2001, "Non-Contact Electron Gun Control of Piezoelectric Polymer Thin Film Structures", *PhD Dissertation*, University of Kentucky, College of Engineering, December.
- Nlemeyer, S. G., Naganathan, N. G., 1995, "Analysis of a piezoceramic XY array actuator", *Proceedings of the 1995 ASME International Mechanical Engineering Congress & Exposition*, San Francisco, CA, Nov. 12-17.
- Paradies, R. , Hertwig, M. Elspass, W. J., 1996, "Shape control of an adaptive mirror at different angles of inclination", *Journal of Intelligent Material Systems & Structures*, v 7 n 2 Mar 1996 p 203-210.
- Paradies, R., and Hertwig, M., 1999, "Shape control of adaptive composite reflectors", *Composites Part B: Engineering*, v 30 n 1 p 65-78.
- Soedel, W., 1993, *Vibrations of Shells and Plate*, New York, Marcel Dekker Inc., p 21.
- Tabata, M., and Natori, M. C., 1996, "Active shape control of a deployable space antenna reflector", *Journal of Intelligent Material Systems & Structures*, v 7 n 2 Mar 1996 p 235-240.
- Tabata, M., Yamamoto, K., Inoue, T., Noda, T., and Miura, K., 1992, "Shape adjustment of a flexible space antenna reflector", *Journal of Intelligent Material Systems & Structures*, v 3 n 4 Oct 1992 p 646-658.
- Tzou, H.S. and Fu, H.Q., 1994, "A Study of Segmentation of Distributed Piezoelectric Sensors and Actuators., Part I: Theoretical Analysis", *Journal of Sound and Vibration*, v 172 n 2 p 250.
- Ueba, M. Tanaka, H. Kawakami, Y., and Ohtomo, I., 1994, "On-board large mesh antenna reflector with high surface accuracy", *Electronics & Communications in Japan, Part I: Communications (English Translation of Denshi Tsushin Gakkai Ronbunshi)*, v 77 n 8 Aug 1994 p 80-89.
- Warren, J. S., 1990, "Modern Optical Engineering: The Design of Optical Systems, 2nd Edition," McGraw-Hill, Inc., *Figure 14.6: Tabulation of typical optical fabrication tolerances*, p 483.
- Yoon, H-S., and Washington, G., 1998, "Piezoceramic actuated aperture antennae", *Smart Materials & Structures*, v 7 n 4 Aug. p 537-542.